

Divergent global precipitation changes induced by natural versus anthropogenic forcing

Jian Liu^{1,2}, Bin Wang³, Mark A. Cane⁴, So-Young Yim³ & June-Yi Lee³

As a result of global warming, precipitation is likely to increase in high latitudes and the tropics and to decrease in already dry subtropical regions¹. The absolute magnitude and regional details of such changes, however, remain intensely debated^{2,3}. As is well known from El Niño studies, sea-surface-temperature gradients across the tropical Pacific Ocean can strongly influence global rainfall^{4,5}. Palaeoproxy evidence indicates that the difference between the warm west Pacific and the colder east Pacific increased in past periods when the Earth warmed as a result of increased solar radiation^{6–9}. In contrast, in most model projections of future greenhouse warming this gradient weakens^{2,10,11}. It has not been clear how to reconcile these two findings. Here we show in climate model simulations that the tropical Pacific sea-surface-temperature gradient increases when the warming is due to increased solar radiation and decreases when it is due to increased greenhouse-gas forcing. For the same global surface temperature increase the latter pattern produces less rainfall, notably over tropical land, which explains why in the model the late twentieth century is warmer than in the Medieval Warm Period (around AD 1000–1250) but precipitation is less. This difference is consistent with the global tropospheric energy budget¹², which requires a balance between the latent heat released in precipitation and radiative cooling. The tropospheric cooling is less for increased greenhouse gases, which add radiative absorbers to the troposphere, than for increased solar heating, which is concentrated at the Earth's surface. Thus warming due to increased greenhouse gases produces a climate signature different from that of warming due to solar radiation changes.

How much will precipitation increase as the world warms as a result of increased greenhouse gases^{2,3,12}? Will the greenhouse-warming-induced precipitation change be different from that induced by natural forcing? Past climate changes might provide guidance. Much has been achieved in the reconstruction of climate from proxy data (tree ring, stalagmites, ice cores, corals, laminated sediments and historical documents) and in numerical simulations of climate change over the past thousand years¹³. There has been great progress in understanding millennial variations of global mean temperature^{14,15} and dynamical modes of climate variability such as the North Atlantic Oscillation and the El Niño–Southern Oscillation (ENSO)⁷, but knowledge of precipitation change remains quite limited and primarily confined to regional scales^{16,17}.

Here we examine differences over the last millennium between global precipitation changes due to natural changes in the solar–volcanic forcing, that is, the sum of the radiative effects of variations in solar irradiance and volcanic aerosols, and precipitation changes resulting from greenhouse-gas forcing. Because proxy data are sparse and the spatial distribution of precipitation is complex, our approach relies on millennial simulations with ECHO-G, an atmosphere–ocean coupled climate model able to reproduce realistic present-day climatology and short-term climate fluctuations (Supplementary Information). The model-simulated present-day precipitation climatology is

comparable to those derived from the state-of-the-art reanalysis data (Supplementary Fig. 1) or the climate models with the best precipitation simulations (see Supplementary Fig. 2). Investigations with this model of various aspects of climate variability including temperature, ENSO and global monsoons^{18–20} have built confidence in the model's credibility for understanding physical processes pertinent to global precipitation change. It is important to note that the simulation we study treats the effect of volcanic aerosol as if it were exactly the same as a reduction in solar radiance²¹. Because it is difficult to extract an unambiguous pattern for the response to greenhouse gases from a simulation that ends in the twentieth century and that also includes solar forcing, we turn to results from a simulation with the same ECHO-G model of the twenty-first century forced by the A1B scenario of greenhouse-gas increases and from a simulation forced by observed greenhouse gases only from 1860–2000 (Supplementary Information).

Strikingly, although the late twentieth century is warmer than the Medieval Warm Period, rainfall is less (Fig. 1). How much global

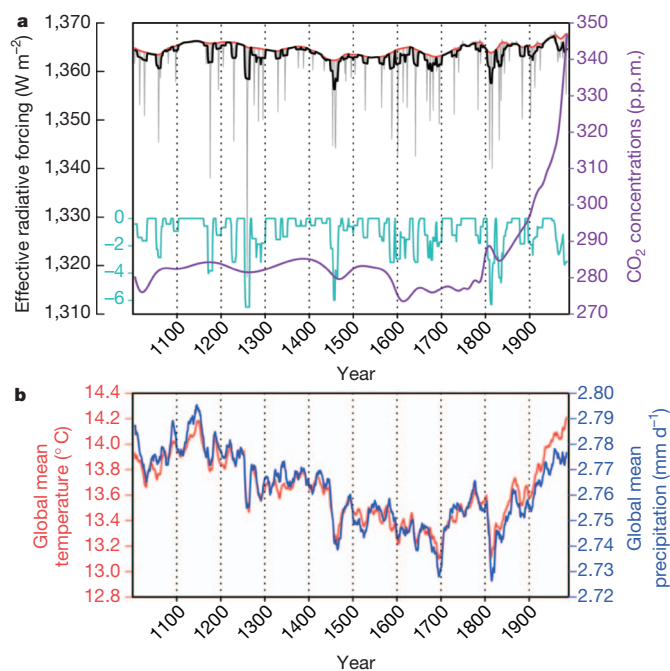


Figure 1 | The external forcing and responses. **a**, The grey line shows the annual mean time series of effective radiative (solar and volcanic) forcing. The red line shows the 11-year running mean time series of solar radiation. The blue line shows volcanic radiative forcing. The black line shows the effective radiative (solar–volcanic) forcing. The purple line shows the CO₂ concentration (right axis). **b**, Shown are the global mean temperature (red), and the global mean precipitation intensity (blue) simulated in the forced run with the ECHO-G model. (p.p.m., parts per million.)

¹Key Laboratory of Virtual Geographic Environment of Ministry of Education, School of Geography Science, Nanjing Normal University, Nanjing 210023, China. ²State Key Laboratory of Lake Science and Environment, Nanjing Institute of Geography and Limnology, Chinese Academy of Sciences, Nanjing 210008, China. ³International Pacific Research Center and Department of Meteorology, University of Hawaii at Manoa, Honolulu, Hawaii 96825, USA. ⁴Lamont-Doherty Earth Observatory of Columbia University, Palisades, New York 10964, USA.

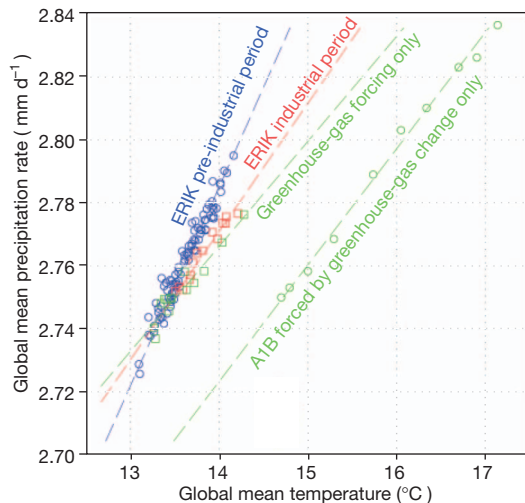


Figure 2 | Scatter plot of decadal means of the global mean precipitation rate versus the global mean temperature, at 2 m above the surface. Blue circles show the millennium simulation (ERIK) for the pre-industrial period (AD 1000–1850), with regression slope $2.1\% \text{ } ^\circ\text{C}^{-1}$ ($0.058 \text{ mm d}^{-1} \text{ } ^\circ\text{C}^{-1}$). Red squares show ERIK for the industrial period (1850–1990), with regression slope $1.4\% \text{ } ^\circ\text{C}^{-1}$ ($0.039 \text{ mm d}^{-1} \text{ } ^\circ\text{C}^{-1}$). Green symbols show two ECHO-G model runs with only greenhouse-gas forcing, with regression slopes $1.2\% \text{ } ^\circ\text{C}^{-1}$ ($0.033 \text{ mm d}^{-1} \text{ } ^\circ\text{C}^{-1}$) (squares) and $1.3\% \text{ } ^\circ\text{C}^{-1}$ ($0.036 \text{ mm d}^{-1} \text{ } ^\circ\text{C}^{-1}$) (circles).

precipitation would increase for a given temperature increase due to global warming has been the subject of intense debate^{2,3}. In the forced millennium simulation (Supplementary Information) this ratio is about $2.1\% \text{ } ^\circ\text{C}^{-1}$ during the pre-industrial period (AD 1000–1850), but only about $1.4\% \text{ } ^\circ\text{C}^{-1}$ during the industrial period (AD 1850–1990) (Fig. 2), a difference that is significant above the 95% confidence level (Supplementary Information). Figure 2 also shows that in two runs with the same model forced only by greenhouse gases (Methods), the ratio is close to but less than that for the industrial period and is again distinct from that in the pre-industrial period when the only

significant forcing is solar. Regional precipitation changes depend on circulation changes and are influenced by local sea surface temperature (SST), and the global precipitation change is not solely dependent on global mean temperature, but what accounts for the difference in this ratio between the Medieval Warm Period and the present?

A good starting point is the tropospheric energy budget: whereas the change in atmospheric water vapour is closely controlled by temperature via the Clausius–Clapeyron relation, precipitation changes are constrained by the energy budget¹². For the troposphere as a whole, the precipitation heating is principally balanced by radiative flux divergence. Thus the total global precipitation is controlled by the difference between the upward radiative flux at the tropopause and that at the earth's surface. All other things being equal, an increase in surface temperature, whether it is due to increased solar flux or increased greenhouse trapping, will increase this flux divergence and hence increase precipitation. However, adding long-wave absorbers to the atmosphere will tend to lessen the difference between the flux at the top and that at the bottom, so the increase in precipitation will be less than if the surface heating results from increased solar radiation¹².

The energy argument can explain the difference in global mean precipitation, but it does not address the spatial distribution of precipitation changes. We first estimate the changes in precipitation and SST by differencing these fields at a time of high solar radiance and little volcanic aerosol (AD 1100–1200, during the Medieval Warm Period; see Fig. 1a) and a time of low solar radiance and high volcanic aerosol (AD 1630–1730, during the Little Ice Age). We take 100-year averages to reduce the influence of higher-frequency natural variability. We will refer to the derived mode as the solar–volcanic mode. It features an enhanced zonal SST gradient in the tropical Pacific Ocean (Fig. 3a) and, as might be expected, the stronger SST gradient is accompanied by stronger easterlies in the equatorial Pacific, and a stronger Walker circulation. It has these features in common with a La Niña event, but the pattern differs in many respects, including having a positive value of the ENSO index NINO3.4 (the SST anomaly averaged over the eastern equatorial box 5°S – 5°N , 120°W – 170°W ; Supplementary Fig. 3), which would be negative for a La Niña event.

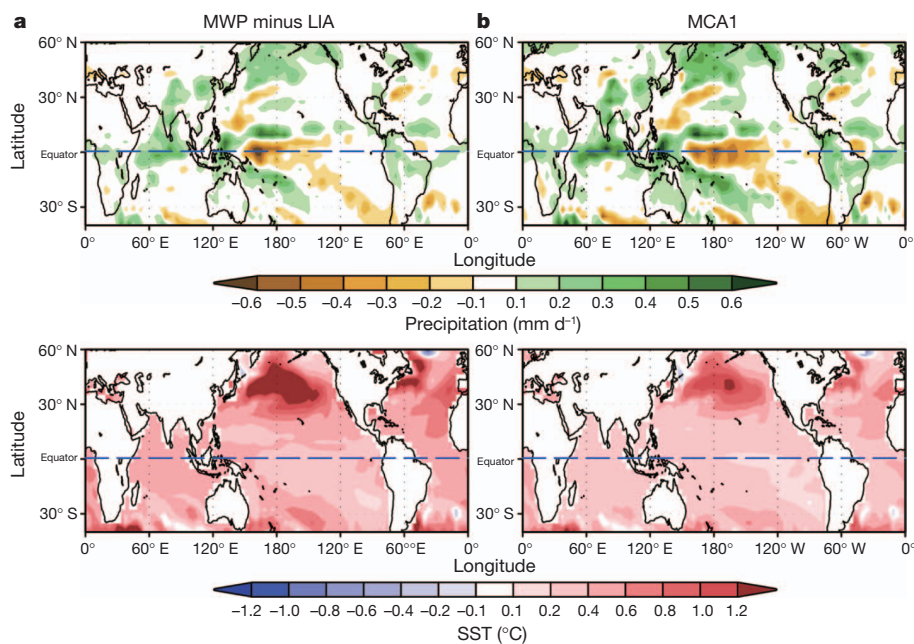


Figure 3 | Spatial patterns of the solar–volcanic forced mode. **a**, The precipitation and SST changes are shown for the Medieval Warm Period (MWP, AD 1100–1200) minus the Little Ice Age (LIA, AD 1630–1730) in response to differences in solar forcing. **b**, The precipitation and SST patterns of the leading maximum covariance analysis mode in the ERIK millennium run

are shown for the period AD 1000–1850, based on 11-year running means after the leading mode of internal variability is removed. (They explain 15.3% and 11.1% of the variance, respectively.) The pattern correlation coefficients between **a** and **b** over the entire domain are 0.92 for precipitation and 0.98 for SST.

We checked this result with a different technique for detecting major patterns of decadal precipitation variations. To focus on the forced response, we first removed the leading internal mode component from the millennium run (Methods and Supplementary Figs 3 and 4) and then applied a maximum covariance analysis (that is, a singular value decomposition²²) to the precipitation and SST fields for the period AD 1000–1850, when the only appreciable forcing is solar–volcanic. The leading coupled spatial patterns of SST and precipitation (Fig. 3b) are markedly similar to the strong gradient patterns of the solar–volcanic mode (Fig. 3a); spatial correlation coefficients are 0.98 and 0.92 for the SST and precipitation fields, respectively. The time expansion coefficients of the precipitation and SST (Supplementary Fig. 5) show a prominent centennial–millennial fluctuation, with a substantial dry and cold epoch during the Little Ice Age (AD 1450–1850), when radiance at the surface due to solar–volcanic forcing is low, and a wet and warm epoch occurring in the Medieval Warm Period (AD 1000–1250), when radiance is high.

The implication that the Medieval Warm Period featured a solar–volcanic pattern (in particular, a stronger zonal SST gradient) but that the global cooling at the Little Ice Age has the opposite pattern agrees with available proxy evidence^{6,7,9} and model results^{23–25}. With increased solar–volcanic forcing the rainfall increases over the climatological ‘wet’ regions, resulting in an overall increase in global mean precipitation (Fig. 3).

To estimate the response induced by greenhouse-gas forcing, we examined two greenhouse-gas-only forcing runs, one for the industrial period (AD 1860–2000) with observed greenhouse-gas concentration as the only forcing, and the other for AD 1990–2100, forced by the A1B scenario of increased greenhouse gases (Supplementary Fig. 6). The resultant trend patterns of SST and precipitation for the two runs are similar except that the A1B run has substantially larger amplitudes than the industrial run, owing to stronger greenhouse-gas forcing. Figure 4a shows the greenhouse-gas mode estimated from the ECHO-G A1B run, which is similar to the Coupled Model Intercomparison Project Phase 5 (CMIP5) multi-model mean projection (Fig. 4b), showing that this pattern in response to greenhouse-gas forcing is common among models. In contrast to the strong zonal SST gradient forced by solar warming, this greenhouse-gas forced mode shows a reduced equatorial Pacific zonal SST gradient. Corresponding to the enhanced and reduced zonal SST gradients, the overall increase of global mean precipitation in the solar–volcanic

mode is larger than that in the greenhouse-gas mode, though the solar–volcanic mode is drier than the greenhouse-gas mode in the central equatorial Pacific. The global total precipitation increase for a given temperature increase due to greenhouse-gas warming (about 1.2% to 1.3% per °C) is about 40% less than that due to solar–volcanic warming (2.1% per °C) (Fig. 2). Of note for societal impacts is that for the solar–volcanic forced mode the rainfall over tropical land increases by 5.5% for a 1 °C increase in global mean temperature, while for the greenhouse-gas forced mode the corresponding increase of 2.4% is less than half of that.

The late twentieth century is warmer than the Medieval Warm Period but the rainfall is less (Fig. 1b), and we argued above that the difference may be attributed to the difference in energy budget constraints when the warming is due to increased greenhouse gases as opposed to solar–volcanic heating. The climate system accommodates the energy budget differences by changing the pattern of global warming. For the same increase in global mean temperature, the solar forced pattern has a stronger SST gradient than the greenhouse-gas forced pattern. Along with the enhanced SST gradient, the Walker circulation strengthens and moisture convergence is concentrated in the Indo-Pacific warm pool region. This wet region gets wetter^{1,2}, augmenting global precipitation.

There is ongoing debate about whether the equatorial Pacific responds to increased heating by enhancing the east–west gradient^{23,24} or reducing it^{2,10,11}. The ‘‘ocean dynamical thermostat’’ theory^{23,24,26} argues that increased heating at the surface warms SSTs in the west more because in the east the heating is countered by upwelling of cold waters from below. The increase in SST gradient gives rise to an enhanced pressure gradient and hence stronger easterly winds and a stronger Walker circulation, which in turn enhance the SST gradient, a mechanism known as ‘‘the Bjerknes feedback’’. The essence of the opposing argument²¹¹ is that because the warming increases the moist static energy in the atmosphere by a greater amount than the energy transports associated with precipitation, the Walker circulation must slow down, so the Bjerknes feedback now implies a weaker SST gradient. The ‘‘ocean dynamical thermostat’’ argument draws support from palaeoclimate proxy data^{6–9,27} and intermediate model simulations^{23,24}. On the other hand, Intergovernmental Panel on Climate Change (IPCC) model projections for the twenty-first century typically show a weaker zonal SST gradient^{1,25}, supporting the weaker Walker argument.

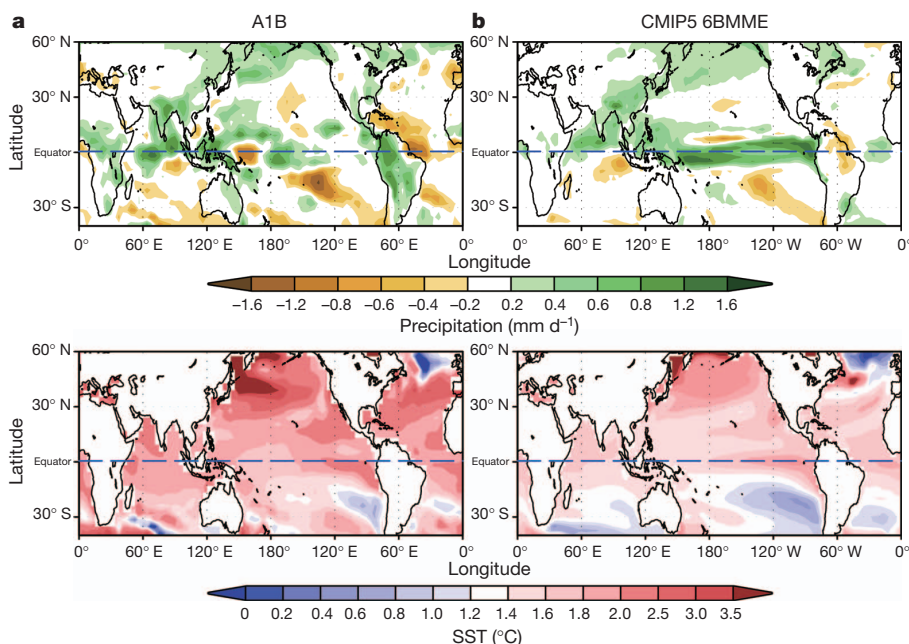


Figure 4 | Comparison of the changes in annual mean precipitation and SST. **a**, The ECHO-G simulated changes under the A1B run forced by greenhouse-gas change only for the period AD 2070–2099 relative to the period AD 1990–2019. **b**, The change in precipitation and SST for the period AD 2070–2099 relative to AD 1980–2005 in the multi-model mean of the six best (6BMME) CMIP5 models forced according to Representative Concentration Pathway 4.5 (a scenario that stabilizes radiative forcing at 4.5 W m⁻² or less in the year AD 2100) forcing (ref. 30). The six best models are the ones with the best simulation of the mean and annual cycle precipitation, as shown in Supplementary Fig. 2. The pattern correlations between **a** and **b** are 0.42 for precipitation and 0.98 for SST.

Figures 3 and 4 show that solar heating led to a stronger SST gradient, whereas greenhouse-gas heating led to a weaker one, demonstrating that there is no contradiction between the palaeoclimate records and the IPCC simulations and that both theories may have a realm of validity. However, neither theory indicates that the outcome should depend on the type of heating. We found that, consistent with the earlier argument for less precipitation with greenhouse-gas forcing than with solar–volcanic forcing, the increase in atmospheric static stability is noticeably greater with greenhouse-gas forcing (Supplementary Fig. 7). The increased atmospheric stability favours a weaker zonal circulation and the accompanying weaker SST gradient characterizing the greenhouse-gas mode. We suggest that although the thermostat and associated stronger gradient pattern dominated in the past when the external warming was solar–volcanic, the weaker gradient pattern associated with greenhouse-gas forcing will dominate future change.

METHODS SUMMARY

Two millennial simulations²⁸ and two greenhouse-gas-only forcing runs with the ECHO-G coupled climate model²⁹ were analysed: (1) a 1,000-year control (free) simulation generated using fixed annually cycling forcing set at present-day values; (2) a forced run, named ERIK, covering the period AD 1000–1990, which is externally forced by solar variability, the effective radiative effects from stratospheric volcanic aerosols, and greenhouse-gas concentrations in the atmosphere, including CO₂ and CH₄, for the period AD 1000–1990; (3) a greenhouse-gas forced run for the period AD 1860–2000 with initial conditions selected from a long pre-industrial control simulation. Nineteen observed greenhouse gases were used, including CO₂, CH₄ and N₂O (ref. 18); and (4) an emissions scenarios (SRES) balance across all sources (A1B) run from AD 1990 to 2100 with 720 p.p.m. stabilization at AD 2100.

To identify the internal decadal variation mode, a principal-component analysis of the 11-year running mean precipitation was performed. To detect major patterns of forced decadal variation, we first removed the leading internal mode component of the precipitation from the ERIK run, and then applied a maximum covariance analysis²² to the precipitation and SST fields for the period AD 1000–1850. To test whether the difference between the two slopes (Fig. 2) was due to sampling errors, we used the Student's *t*-test (it was not). Further details are given in the Supplementary Information.

Received 21 September; accepted 8 November 2012.

- Meehl, G. A. *et al.* Global climate projections. In *Climate Change 2007: The Physical Science Basis. Contribution of Working Group I to the Fourth Assessment Report of the Intergovernmental Panel on Climate Change* (eds Solomon, S. *et al.*) 747–845 (Cambridge Univ. Press, 2007).
- Held, I. M. & Soden, B. J. Robust responses of the hydrological cycle to global warming. *J. Clim.* **19**, 5686–5699 (2006).
- Wentz, F., Ricciardulli, L., Hilburn, K. & Mears, C. How much more rain will global warming bring? *Science* **317**, 233–235 (2007).
- Ropelewski, C. F. & Halpert, M. S. Global and regional scale precipitation patterns associated with the El Niño/Southern Oscillation. *Mon. Weath. Rev.* **115**, 1606–1626 (1987).
- Ropelewski, C. F. & Halpert, M. S. Quantifying Southern Oscillation–precipitation relationships. *J. Clim.* **9**, 1043–1059 (1996).
- Adams, J. B., Mann, M. E. & Ammann, C. M. Proxy evidence for an El Niño-like response to volcanic forcing. *Nature* **426**, 274–278 (2003).
- Cobb, K. M., Charles, C. D., Cheng, H. & Edwards, R. L. El Niño–Southern Oscillation and tropical Pacific climate during the last millennium. *Nature* **424**, 271–276 (2003).
- Mann, M. E., Cane, M. A., Zebiak, S. E. & Clement, A. Volcanic and solar forcing of the tropical Pacific over the past 1000 years. *J. Clim.* **18**, 447–456 (2005).
- Mann, M. E. *et al.* Global signatures and dynamical origins of the little ice age and medieval climate anomaly. *Science* **326**, 1256–1260 (2009).
- Meehl, G. A. & Washington, W. M. El Niño like climate change in a model with increased atmospheric CO₂ concentration. *Nature* **382**, 56–60 (1996).
- Vecchi, G. A. *et al.* Weakening of tropical Pacific atmospheric circulation due to anthropogenic forcing. *Nature* **441**, 73–76 (2006).
- Allen, M. R. & Ingram, W. J. Constraints on future changes in climate and the hydrologic cycle. *Nature* **419**, 224–232 (2002).
- Mann, M. E. Climate over the past two millennia. *Annu. Rev. Earth Planet. Sci.* **35**, 111–136 (2007).
- Mann, M. E., Bradley, R. S. & Hughes, M. K. Northern hemisphere temperatures during the past millennium: inferences, uncertainties, and limitations. *Geophys. Res. Lett.* **26**, 759–762 (1999).
- Moberg, A., Sonechkin, D. M., Holmgren, K., Datsenko, N. M. & Karlen, W. Highly variable northern hemisphere temperatures reconstructed from low- and high-resolution proxy data. *Nature* **433**, 613–617 (2005).
- Pauling, A., Luterbacher, J., Casty, C. & Wanner, H. 500 years of gridded high resolution precipitation reconstructions over Europe and the connection to large scale circulation. *Clim. Dyn.* **26**, 387–405 (2006).
- Dore, M. H. I. Climate change and changes in global precipitation patterns: what do we know? *Environ. Int.* **31**, 1167–1181 (2005).
- Min, S. K. & Hense, A. A Bayesian assessment of climate change using multimodel ensembles. Part I: global mean surface temperature. *J. Clim.* **19**, 3237–3256 (2006).
- Rodgers, K. B., Friedrichs, P. & Latif, M. Tropical Pacific decadal variability and its relationship to decadal modulations of ENSO. *J. Clim.* **17**, 3761–3774 (2004).
- Liu, J. *et al.* Centennial variations of the global monsoon precipitation in the last millennium: results from the ECHO-G model. *J. Clim.* **22**, 2356–2371 (2009).
- von Storch, H. *et al.* Reconstructing past climate from noisy data. *Science* **306**, 679–682 (2004).
- Wallace, J. M., Smith, C. & Bretherton, C. S. Singular value decomposition of wintertime sea surface temperature and 500-mb height anomalies. *J. Clim.* **5**, 561–576 (1992).
- Clement, A. C., Seager, R., Cane, M. A. & Zebiak, S. E. An ocean dynamical thermostat. *J. Clim.* **9**, 2190–2196 (1996).
- Cane, M. A. *et al.* 20th century sea surface temperature trends. *Science* **275**, 957–960 (1997).
- Vecchi, G. A., Clement, A. & Soden, B. J. Examining the tropical Pacific's response to global warming. *Eos* **89**, 81 (2008).
- Bauer, E., Claussen, M. & Brovkin, V. Assessing climate forcings of the Earth system for the past millennium. *Geophys. Res. Lett.* **30**, 1276 (2003).
- Emile-Geay, J., Seager, R., Cane, M. A., Cook, E. R. & Haug, G. H. Volcanoes and ENSO over the last millennium. *J. Clim.* **21**, 3134–3148 (2008).
- Zorita, E., Gonzalez-Rouco, J. F., von Storch, H., Montavez, P. & Valero, F. Natural and anthropogenic modes of surface temperature variations in the last thousand years. *Geophys. Res. Lett.* **32**, L08707 (2005).
- Legutke, S. & Voss, R. *The Hamburg Atmosphere–Ocean Coupled Circulation Model ECHO-G*. Technical Report 18, 1–62 (German Climate Computer Center (DKRZ), 1999).
- Lee, J. Y. & Wang, B. Future change of global monsoon in the CMIP5. *Clim. Dyn.* doi:10.1007/s00382-012-1564-0 (2012).

Supplementary Information is available in the online version of the paper.

Acknowledgements This work was supported by the National Basic Research Program (award numbers 2010CB950102 and XDA05080800 to J.L.) and Natural Science Foundation of China (award number 40871007 to J.L. and B.W.). B.W. and J.-Y.L. acknowledge the Global Research Laboratory (GRL) Program from the Korean Ministry of Education, Science and Technology (MEST, 2011-0021927). M.A.C. was supported by grant DE-SC0005108 from the Department of Energy and NOAA grant NA08OAR4320912. B.W., S.-Y.Y. and J.-Y.L. acknowledge support from the International Pacific Research Center, which is funded jointly by JAMSTEC, NOAA and NASA. We thank E. Zorita for providing ECHO-G millennium run data, and A. Hense and S.-K. Min for providing ECHO-G A1B and greenhouse-gas run data.

Author Contributions J.L. initiated the research. J.L., B.W. and M.A.C. contributed to the research and wrote the manuscript. S.-Y.Y. and J.-Y.L. made analyses and contributed to the graphics.

Author Information Reprints and permissions information is available at www.nature.com/reprints. The authors declare no competing financial interests. Readers are welcome to comment on the online version of the paper. Correspondence and requests for materials should be addressed to M.A.C. (mcanec@leao.columbia.edu) or J.L. (jliu@njnu.edu.cn).